# Lessons learnt during the first Quality Assurance exercise of the ACTRIS high-power lidars

L. BELEGANTE[1], C. TALIANU[1,2,*], A. NEMUC[1], V. NICOLAE[1], G. CIOCAN[1], F. TOANCA[1], O. G. TUDOSE[3], C. RADU[1], D. NICOLAE[1]

[1]*National Institute of Research and Development for Optoelectronics - INOE 2000, Remote Sensing Department, 409 Atomistilor street, Magurele, PO Box MG-05, Magurele, 077125, Romania*

[2]*Institute of Meteorology and Climatology, Department of Water, Atmosphere and Environment, University of Natural Resources and Life Sciences, Gregor-Mendel Street 33, Vienna, A-1180, Vienna, Austria*

[3]*INOESY S.R.L., 8 Fdc. Mestecanis Street, 707410, Valea Lupului, Iasi, Romania*

This paper presents the results of the first Quality Assurance (QA) exercise under the ATMO-ACCESS pilot, aimed at calibrating and validating ATLID onboard the EarthCARE satellite. The exercise involved 24 high-power lidars from ACTRIS and EARLINET, across 12 countries. Typical problems of the lidar systems, limitations in terms of performances and estimation of the correction factors were extracted from the specific quality assurance tests. Key findings include the identification of typical system limitations and correction factors. Most lidar systems showed full overlap altitudes between 200 and 1000 m, though additional near-range telescopes may be needed to meet ACTRIS standards. The maximum product height retrieved from the tests indicate that the 532 nm and 355 nm channels perform better, with mean maximum altitudes around 16 km, while the 1064 nm channel is limited to 7.4 km. Polarization calibration revealed systematic errors below 0.005 for most of the instruments, supporting reliable aerosol typing, although some instruments showed higher errors.

(Received October 3, 2024; accepted October 7, 2024)

*Keywords:* Lidar, Aerosols, Quality assurance, Systematic bias, Measurement uncertainty

## 1. Introduction

Our air environment is continually changing, owing to direct anthropogenic emissions and climatic feedback processes [1]. Short-lived Atmospheric Constituents (SLACs) regulate the Earth's climate and have an impact on air quality, as well as the health of humans and ecosystems. Their concentration is determined not only by the intensity of primary emissions (sources) and removal mechanisms (sinks), but also by a complex collection of secondary reactions that are still poorly understood and may develop in the next decades as a result of climate change [1-4].

The movement of the Earth's atmosphere is an important aspect in all research involving the characterisation of our planet. There are other tracers that may be used to indicate how the atmosphere moves, but aerosols are one of the best [5-7]. Their chemical composition does not change fast due to chemical reactions. Their physical and optical qualities change extremely slowly. Many investigations on the interchange of air between the troposphere and stratosphere, the dynamics of the polar regions, and stratospheric transport from low to high latitudes have demonstrated that aerosol measurements are appropriate for these goals [8-10].

The presence of aerosols in the atmosphere has both direct and indirect effects on the climate and the Earth's radiation budget. Aerosols scatter sunlight directly back into space, whereas the presence of aerosols in the lower atmosphere can alter the size of cloud particles, affecting how clouds reflect and absorb sunlight, and therefore modifying the Earth's energy budget [11-12]. Since 1986, investigations on the ozone hole have revealed major reactions taking place on aerosol surfaces (the heterogeneous chemistry), resulting in the depletion of stratospheric ozone over Antarctica [13-15]. The science community recognizes that airborne pollution particles in the Earth's atmosphere have an effect on climate equivalent in scale to growing quantities of atmospheric gases.

The uncertainty around aerosol effect can be larger than those seen in climate models [1]. So, improving the performance of climate models is a major problem since they do not provide a realistic conclusion on how aerosols may affect the climate. Scientists require and seek very precise and thorough aerosol observations.

ACTRIS (Aerosol, Clouds and Trace gases Research Infrastructure) is a new European Research Infrastructure consortium for short-lived atmospheric elements that promotes basic research and excellence in Earth system monitoring [16][17]. The major goal of ACTRIS is to provide high-quality integrated datasets in the field of atmospheric sciences for scientists working in atmospheric research and beyond.

The Center for Aerosol Remote Sensing (CARS) is one of six ACTRIS Topical Centres, being responsible for the calibration and quality assurance of the lidar and photometer measurements across the continent. Its goal is to accurately measure the optical characteristics of tropospheric and low stratospheric aerosols and deduce their microphysical properties. CARS incorporates aerosol

column and aerosol profiling measurement methods, as well as their synergistic applications at ground level [18].

Because of hardware changes (for example, laser power and sounding wavelengths), the data products obtained from various measuring techniques are fundamentally different. Aerosol layering and attenuated backscatter at one wavelength are now achieved using automatic low-power lidars and ceilometers (ALC) [19]. Aerosol high-power lidars (AHL) are aerosol lidars that, due to their increased power, may offer more quantitative information regarding aerosol optical characteristics than the ALC. AHL, in particular, was used to profile aerosol optical properties (aerosol backscatter coefficient, aerosol extinction coefficient, and aerosol linear depolarization ratio) at one or more wavelengths, allowing for the subsequent calculation of several spectral parameters (Angstrom exponents, lidar ratios) of the lofted aerosol layers [20-23], and thus aerosol typing [24-27].

A lidar is a very sophisticated and technically difficult equipment. Measurement of atmospheric lidar signals requires high-speed electronics with an extraordinarily broad bandwidth and dynamic range. Especially for tropospheric aerosol research, weak lidar signals cannot be averaged over long periods of time (hours) and must be measured during the day against a high daylight background in order to use synergy with other measurement platforms such as sun-photometers and airborne measurement, putting high demands on the optical design of the transmitter and receiver [28][29]. The wavelengths usually utilized are determined by the availability of a high-power laser source, primarily the NdYAG laser, with a wavelength range that exceeds commercially available optics [29]. At the same time, achieving the requisite SNR necessitates compact photo-detectors and big telescopes for weak signals, posing a design problem for the receiver's optical section [29]. Furthermore, because the lidar measurement targets the wide-stretched atmosphere, there is no calibration standard for lidar signals, with the exception of the distant range, where clean air (Rayleigh scattering) can be employed [28][30-32]. However, extremely tiny signal variations caused by electronic distortions, atmospheric variance, or inadequacies in the transmitter and receiver optics can significantly alter lidar signals and calibration in clean air ranges and must therefore be identified [28].

Lidar systems may have intrinsic flaws, but they are also vulnerable to environmental factors such as temperature variations, humidity, vibration and movement, as well as user errors [28][33]. As a result, we require a set of tools that allows a common lidar operator to ensure that the lidar is functioning properly. However, there is no standard definition of a "proper operation" yet.

The collection, harmonisation, and development of standards and calibration techniques began under the umbrella of EARLINET and ACTRIS, including the calculation of Rayleigh scattering coefficients, Rayleigh-fit tests, trigger delay determination, telecover tests, dark signal subtraction, specialised lidar pulse generator to estimate the performance of the electronics, and polarisation calibration, primarily to avoid signal disturbance. These are intended to serve as a foundation for the ACTRIS high-power aerosol lidars' QA/QC program [16].

ACTRIS Centre for Aerosol Remote Sensing (CARS) provides QA tools which enable to determine the uncertainty of the signals at all wavelengths individually and of their ratios (lidar ratio, linear depolarisation ratio) over the whole detection range from 200 m to 15 km, which are the basis of an error estimation of the final lidar products, and develops methods and recommendations to improve the quality.

Several QA tools were developed in the former EARLINET-ACTRIS projects [28]. They are employed at CARS and further developed to include more details, but must also consider future lidar developments as, e.g., the High-Spectral-Resolution-Lidar (HSRL) technique and the circular depolarisation ratio.

## 2. Instruments and methodology

A typical ACTRIS high-power aerosol lidar is based on a commercial and hence affordable Nd: YAG laser with its three emitted wavelengths 355, 532, and 1064 nm [16]. At these wavelengths the lidar measures elastically backscattered photons from which the aerosol backscatter coefficient can be deduced with an assumed ratio between extinction and backscatter, i.e. the so called lidar-ratio. Because of the daylight background, the output pulse power must be high and can range from 20 mJ to 600 mJ per pulse at 10 to 30 Hz repetition rate in order to achieve a good signal to noise ratio. The measurement range is nowadays typically from 500 m above ground (a.g.) to 15 km a.g.. During night it is possible to measure weaker signals from inelastically backscattered photons from atmospheric gases at vibrational or rotational shifted Raman wavelengths (e.g. 387, 408, 607 nm), from which – together with the elastic signals - the aerosol extinction coefficient can be retrieved. For these measurements large telescopes are desirable, wherefore typical telescope diameters are in the range from 100 to 400 mm.

An optimal lidar setup would include a small telescope for the elastic signals and a large telescope for the inelastic signals, but most present lidars have only one large telescope to reduce manufacturing costs. Furthermore, the depolarisation of the linearly polarised laser beam at the elastic wavelengths due to aerosols can be measured to gain more information about the type of the aerosol particles.

At present, a typical lidar includes three channels at the elastic wavelengths, two channels at the inelastic wavelengths, and two channels to measure the depolarisation at one wavelength. These are the so called 3+2+1 lidars [34]. Such a multi-wavelength polarisation diversity lidar system for night time and daytime measurements comprises a complex wavelength separation unit.

In future we expect 3+2+3 and even 3+3+3 setups, which will increase the complexity. Furthermore, it is highly desirable and expected that the detection range will be extended down to 200 m a.g. to include this part of the boundary layer which often contains most of the aerosol.

This adds another order of magnitude to the dynamic range of the signals and much higher demands on the mechano-optical design of the lidar with more sources for larger systematic errors. The 200 m limit is based on the current requirements provided by ACTRIS CARS and stems from expert analysis of existing technical solutions and the operational limitations of current lidar instruments [16].

Due to the lack of an absolute calibration reference for lidar signals especially in the lower atmosphere, such systematic errors are very often not noticed at all. These errors can lead to uncertainties of the aerosol backscatter and extinction coefficients in the order of 50% and of the linear depolarisation ratio in the order of typically 0.05 [28][35]. While the errors in the scattering coefficients are directly related to the aerosol optical thickness and their climate effect and health impact and affect the synergetic products with other remote sensors as sun-photometers and radars (CloudNet stations) and on satellites, the errors in the linear depolarisation ratio and in the lidar ratio render the aerosol typing very uncertain [15] [21] [22].

The basis of quality criteria for lidar signals and their products are the error bars. Errors of measuring instruments can be determined by measurements of calibration standards or by comparison with a reference instrument. Due to the extent of the measurement object of lidars, which is the atmosphere, calibration standards for lidars cannot be fabricated. Comparisons with reference lidar systems are laborious and expensive and cannot be performed as often as necessary. Furthermore, such comparisons suffer from the fact that the measurement target, i.e. the atmosphere, is temporally and spatially inhomogeneous. Therefore, techniques have been developed to indirectly determine contributions from different error sources of the lidar system. These techniques are described in [33][36][37], which can be applied by the lidar operators. Because the individual error sources are of very different nature, and several are even unknown yet, their combination into final error bars is very complex and a general procedure for that does not exist yet.

The present QA tools comprise mathematical data analysis techniques as the Rayleigh- or signal-fit searcher (SFITS), the polarisation calibration (Δ90-calibration) and detection and correction of the polarisation dependent systematic errors (GHK-correction), and instrumental techniques as the analysis of analogue signal distortions, the determination of the lidar alignment and of the near and far range overlap function, as well as the detection of faults in the mechano-optical lidar setup [38].

An extensive exercise to collect and analyse QA tests for the aerosol high-power lidar was organized between August 2023 and August 2024. Twenty-four lidar stations, out of which 18 ACTRIS and 6 non-ACTRIS, have submitted at least one set of QA tests to CARS. Each set of tests has been analysed by CARS experts using the ATLAS (Automated Lidar Analysis Software) [39]. In total, 31 reports have been issued. In some cases, CARS requested the re-submission of tests because the atmospheric conditions proved to be improper for the analysis.

Each report includes the following information: a) parameters used as inputs for the processing chain (minimum product height, maximum product height, dead time values for each channel, first signal rangebin); b) parameters describing the performances of the instrument (Volume Linear Depolarization Ratio - VLDR systematic error); c) recommendations for optimization of the instrument or conditions of the tests. The first set of parameters is further used to setup, for that particular lidar, the operational configurations in the Single Calculus Chain (SCC), the centralized processing software [40][41]. The stability of these parameters over time (i.e. from one QA exercise to the next) gives additional information on the stability of the instrument but also on how well the instrument is operated.

The Quality Assurance tests considered in this analysis are shortly described in sections 2.1 – 2.5.

### 2.1. Telecover test

Deviations of near-range signals from various portions of the telescope, as well as comparisons of such deviations among lidar channels, can provide the distance of full overlap and plausible explanations for departures from the ideal scenario.

The telecover test evaluates the performance of lidar systems by analyzing deviations in near-range signals collected from different parts of the telescope. By comparing these deviations across various lidar channels and against theoretical ray-tracing simulations, the test helps determine the distance of full overlap and identifies potential reasons for deviations from ideal performance. In the near range, where calibration methods are limited and clean air conditions are rarely present, any shortcomings in optical and opto-mechanical design, or misalignments, can significantly impact signal accuracy. Ideally, the normalized signals from all telecover tests should match, indicating consistent performance across the system, except for the overlap range, which can then be accurately assessed under stable atmospheric conditions.

The telescope can be covered in such a way that only specific sections are utilized. The Quadrant-test divides the telescope into four sections (North, East, South, and West), while the Octant-test further splits these quadrants into eight sections, making them suitable for both co-axial and bi-axial lidar instruments. The Ring-test, on the other hand, is specifically designed for co-axial lidar instruments. With an ideal lidar system, the normalized signals from all telecover tests must match, with the exception of the overlap range, which may be checked, assuming constant air conditions during testing.

### 2.2. Polarization calibration

The volume linear depolarization ratio profile (VLDR) and particle linear depolarization ratio profile (PLDR) must be calculated using polarization sensitive lidar channels that have been calibrated. To execute a polarization calibration, the AHL must be equipped with a polarization calibration module. The calibration of polarization channels is unique to each lidar system, however the fundamental concepts are comparable for the majority of sensors. The polarization

channels are calibrated by first analyzing the observed calibration factor and then making any required modifications to lower the instrument's contribution.

The 45° calibration is a viable approach for calibrating polarization measurements. This calibration rotates the polarization analyzer (PBS and PMTs) by 45° with regard to the laser's polarization plane to equalize light intensity in the cross and parallel channels. When comparing calibration signals, the ratio of sent to reflected signals reveals the role of optics and electronics in the lidar receiving unit. The major source of error in this type of calibration is the accuracy, which defines the 45° rotation with regard to the PBS's real zero point. A more sophisticated option is to conduct two following measurements by rotating the polarization analyzer at ±45° from the default measuring position [42]. This calibration is known as the "±45° calibration". The calibration constant is calculated by taking the geometric mean of two ±45° readings. The two measurements are intended to compensate for each other, even when the 45° rotation error is significant in comparison to the PBS's original zero position [43].

For ±45° calibration, the initial zero position reference is not necessary. Instead, a more general method is to conduct two consecutive measurements by rotating the polarization analyzer with an identical 90° difference between them. The "Δ90° calibration" yields results comparable to the ±45° calibration, but with more precision. The ±45° calibration is similar to the Δ90° rotation calibration, except it only requires a precise 90° angle between the two observations.

The polarization calibration modules might be based on a variety of technical solutions: a) Mechanical rotator; b) half-wave plate rotator; c) polarizer filter. To accomplish Δ90° calibration, the lidar operator can use a mechanical rotator (holder) that rotates optical components at set angles. This calibrator will be known as the "Δ90° mechanical rotation calibrator". A half-wave plate (HWP) can correctly rotate emitted or collected light at Δ90°, resulting in a comparable technique with the same output. A third way to Δ90° calibration involves rotating an extra linear polarizer at defined angles. The Δ90° rotation will be performed using an extra linear polarizer.

### 2.3. Rayleigh fit test

The only absolute calibration of lidar signals is the comparison of signals in clean air ranges to signals estimated from air density and temperature profiles obtained from radiosondes. To calibrate lidar signals using Rayleigh (molecular) backscatter signals, optoelectronic detecting devices must have a wide dynamic range.

The Rayleigh-fit normalizes the range corrected lidar signal to the computed attenuated molecular backscatter coefficient (βm attn, Rayleigh signal) in a range where we assume clean air without particles, and the calculated signal matches the lidar signal within the noise limits [28].

The Rayleigh fit test is an extended conventional lidar measurement done in clear atmospheric circumstances (no cirrus clouds). The test must be carried out with the same lidar setup as under regular measurement conditions. The Rayleigh fit test signals are preprocessed similarly to standard measurements.

### 2.4. Zero bin test

A trigger delay between the actual laser pulse production and the supposed zero range of the signal recording (zero bin) might result in significant inaccuracies in the near-range signal up to roughly 1 km. The inversion of Raman signals, in particular, can be considerably affected since the signal slope in the near range changes significantly when the zero-bin for range correction is altered. As a result, it is worthwhile to make an effort to ensure that the zero-bin is indeed located where we believe it is [28].

When pre-trigger samples are captured, the zero-bin is immediately identifiable due to the signal peak from stray light diffusely reflected from the laboratory walls. Because the distance to the laboratory walls is not clearly defined, a diffuse scattering target obstructing the laser path can be employed in conjunction with a tiny hole aperture above the telescope to reduce the signal height within the detection range of the detectors.

If no pre-trigger samples are acquired, the zero-bin can be identified using a near-range target at a known distance from the lidar. Alternatively, the appropriately attenuated outgoing laser pulse can be fed into an optical fiber of suitable length, with the fiber output positioned at the aperture of the telescope. With this, a signal pulse may be detected with a delay $dt = s / v = s / c * n$ with regard to the outgoing laser pulse, where c is the speed of light in vacuum and v is the speed of light in the fiber with refractive index n at the receiver channel wavelength [28].

### 2.5. Extended dark signal measurement test

Signal distortions that are independent of the lidar signal but synchronized with laser repetition can be evaluated using a technique known as dark measuring. The detected dark signals, which do not include air backscatter from the laser, can be subtracted from the standard lidar signals in the same way as the skylight background or the analogue DC-offset are, but in a range-dependent manner [28]

The dark measurement is similar to a standard measurement, with a laser and a Q-switch trigger, but with a totally covered telescope or a shutter obstructing the optical path within the receiver, so that no light from the atmosphere or backscattered laser pulse is captured by the detectors. In such signals, we can witness interferences from electro-magnetic laser pulses or other electrical interferences that are synchronized to the laser trigger, as well as residual analogue low frequency noise that can never be totally eliminated by spatial or temporal averaging.

Because there are several causes of such disturbances with varying impacts on averaged lidar signals, we presently lack a defined approach for dark measurements and hence cannot use them to evaluate lidar signal quality in a consistent manner. However, if the signal distortions

remain stable after adequate temporal averaging of the dark measurement, that is, they will not change with more temporal averaging, the dark signals can be eliminated from the atmospheric signals to increase their accuracy. The test is mostly used for analogue channels.

## 3. Results and discussion

### 3.1. Full overlap

The results for the telecover indicate two distinct cases. The upper figure shows a non-optimal scenario, where significant atmospheric instability is detected between 800 m and 1500 m, particularly in the East and West sectors. In contrast, the lower figure illustrates an improved Quality Assurance (QA) telecover test (Fig. 1).

Each figure contains three plots: the left plot presents the four signals for each sector (North, East, South, and West), while the middle plot displays the normalized signals, facilitating comparison across sectors. The right plot shows the relative sector deviation, with limits set at 0.05. To reduce atmospheric variability, the test was performed in five iterations, and the shaded areas in each signal plot represent the signal variability for each sector during these iterations.

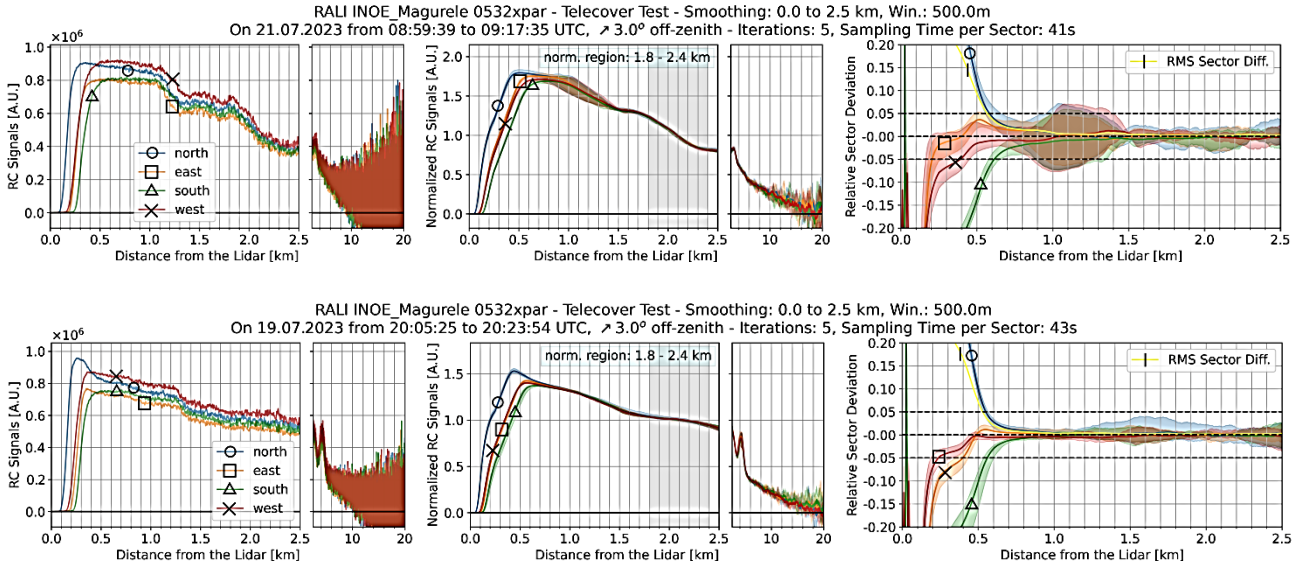


*Fig. 1. Results for the telecover test, RALI instrument at 532 nm. Upper: non-optimal atmospheric conditions – high variability around 1 km; Lower: optimal atmospheric conditions (color online)*

The two examples show results obtained using the Raman lidar instrument at the Măgurele site (RALI) for the 0532xpar channel. In the non-optimal case (upper figure), the full overlap distance is observed at an altitude of 600 m, whereas in the improved case (lower figure), this altitude decreases to 500 m. This reduction in full overlap height in the second case suggests a more efficient alignment and optimization of the system during the telecover test.

The two examples emphasize the significant impact of atmospheric variability on the assessment of full overlap, reinforcing the need for conducting the telecover test under stable atmospheric conditions (low variability). To ensure reliable results, it is recommended to perform at least 3-5 interleaved N-E-S-W iterations for each test. This approach minimizes the influence of atmospheric fluctuations and provides a more accurate evaluation of the lidar system's performance.

The statistical analysis of the 24 AHLs shows that the mean overlap altitude for all three channels is around 500 m. Variability is most pronounced in the 1064 nm channel, where some lidar systems exhibit full overlap altitudes reaching up to 1500 m (Fig.2).

The data also highlights that most lidar systems would not meet the ACTRIS minimum requirement, which specifies that full overlap should be achieved below 300 m. This suggests that many instruments will require additional near-range telescopes to properly capture the lower regions of the Planetary Boundary Layer (PBL), where critical surface-atmosphere interactions take place. The 1064 nm channel, in particular, shows the widest distribution of full overlap altitudes, indicating a greater spread in performance across instruments at this wavelength.

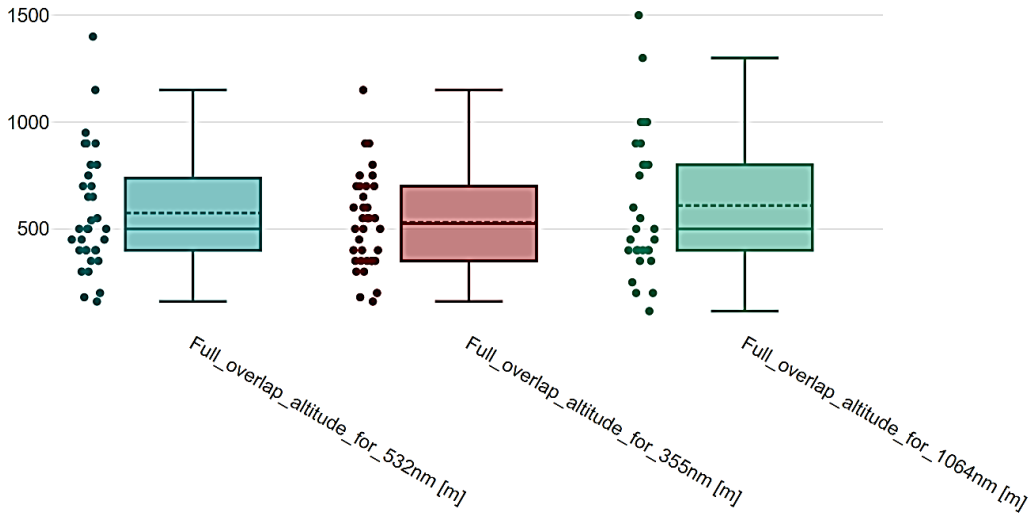


*Fig. 2. Statistical analysis of the full overlap region at 532 nm,355 nm and 1064 nm (color online)*

### 3.2. Maximum altitude height

The Rayleigh Fit results were used to assess the maximum altitude height for the 532 nm and 355 nm photon counting channels, using both the Alpha and RALI lidar instruments at Magurele [44][45][46][47] (Fig.3). The left plot shows the lidar signal normalized to the Rayleigh molecular signal, while the right plot displays the relative difference between the lidar signal and the Rayleigh signal.

In the first example, significant deviations from the expected Rayleigh signal occur above 16 km, indicating that the retrievals at these altitudes may be unreliable due to potential instrument misalignment or atmospheric variability. For the second example, the signal-to-noise ratio (SNR) drops above 9 km, making it difficult to assess the maximum altitude range beyond this height. To improve the SNR and provide more reliable results, it is recommended that the Rayleigh test be extended over several hours, particularly during clear atmospheric conditions.

The third and fourth examples show ideal results for both the 532 nm and 355 nm channels, with good agreement between the lidar signal and the Rayleigh molecular signal. In the third case, the normalization region was determined between 11 and 14 km, and the maximum reliable altitude height was estimated at 14.1 km. In the final example, normalization was extended up to 20 km, providing reliable signal retrievals up to this altitude, reflecting ideal atmospheric conditions and instrument performance.

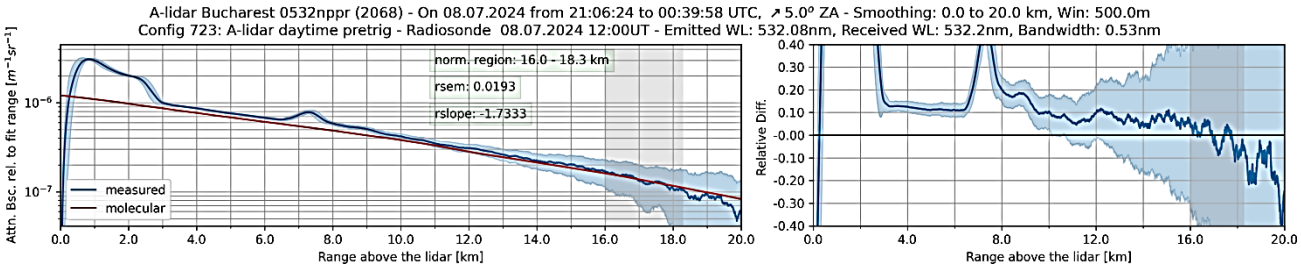


*(a)*

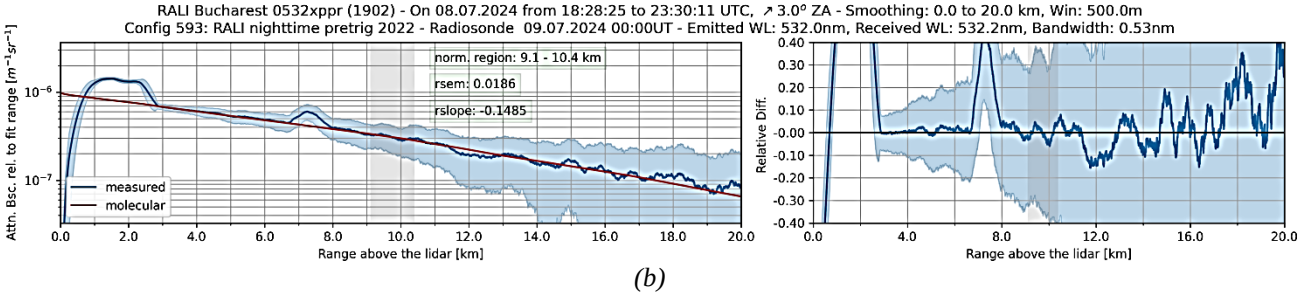


*(b)*

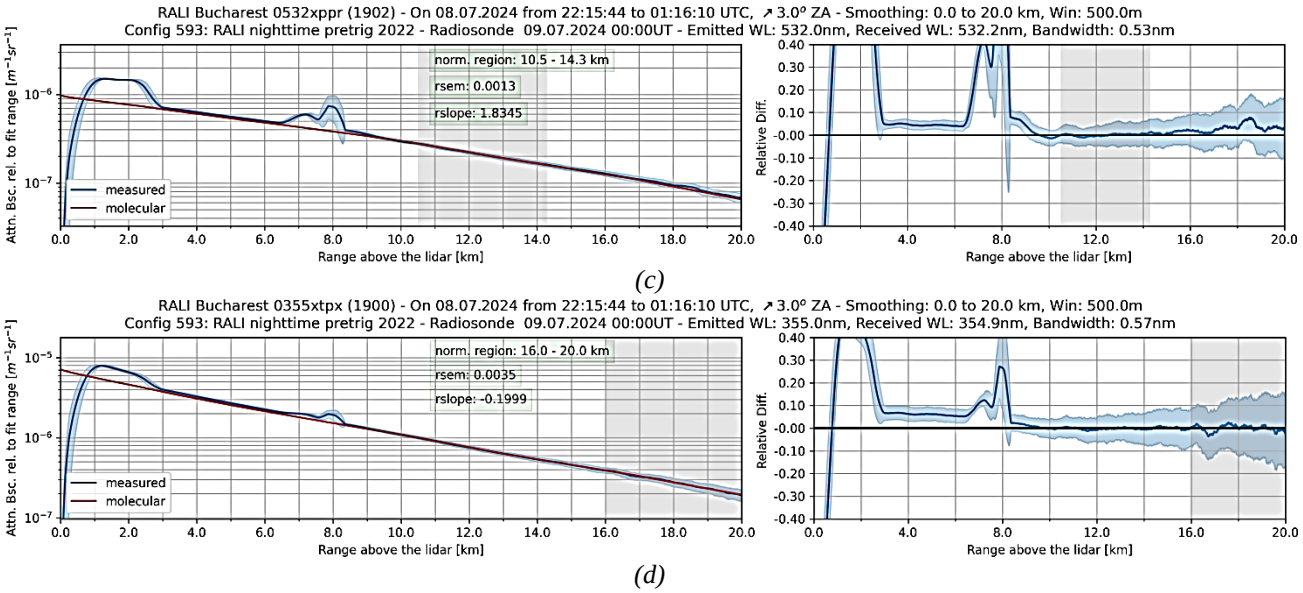


*Fig. 3. Results for the Rayleigh fit test, collected using two lidar instruments at 532 nm and 355 nm. a: significant deviations in the far range (16 – 20 km); b: low SNR for upper altitudes (from 10 km); c: ideal results for 532 nm – good agreement up to 20 km (aerosol layers at 18 km); d: ideal results for 355 nm – good agreement up to 20 km (color online)*

The statistical analysis of the Maximum Altitude Height for the 532 nm, 355 nm, and 1064 nm channels of the 24 AHLs highlights a significant difference in performance between these wavelengths (Fig.4). For the 532 nm and 355 nm channels, the maximum altitude height often reaches up to 20 km in several cases, with a mean maximum altitude of 16 km for the 532 nm channel and 15.7 km for the 355 nm channel. These results suggest that both channels provide reliable data for atmospheric studies at high altitudes, demonstrating strong signal quality and detection range.

In contrast, the performance of the 1064 nm channel is notably lower, with the maximum altitude height typically limited to 13 km, and a mean value of just 7.4 km. This significant difference in performance between the 1064 nm channel and the other two wavelengths could be attributed to the technical limitations of current detection modules. While photomultiplier tubes (PMTs) operating in photon-counting mode are commonly used for the 532 nm and 355 nm channels, the 1064 nm channel typically relies on avalanche photodiodes (APDs) in analog detection mode. The analog detection method increases the likelihood of signal distortions, reducing the signal-to-noise ratio (SNR) and limiting the overall detection range for the 1064 nm channel.

These findings underscore the need for improved detection technologies for the 1064 nm wavelength to bring its performance closer to that of the 532 nm and 355 nm channels, particularly in applications requiring high-altitude atmospheric observations.

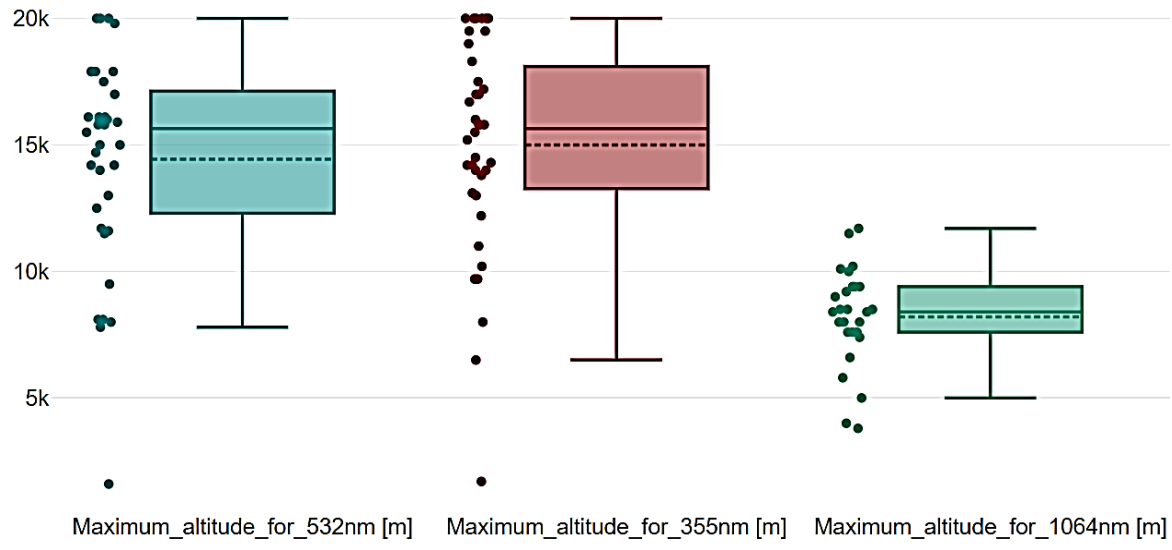


*Fig. 4. Statistical analysis of the maximum altitude region at 532 nm, 355 nm, and 1064 nm (color online)*

### 3.3. Polarization calibration

The Polarization calibration tests conducted for the 355 nm polarization channels of the Alpha lidar instrument reveal important insights into the instrument's performance. Two examples are analyzed, with results presented in terms of gain ratio profiles and Volume Linear Depolarization Ratio (VLDR) profiles (Fig.5).

In the first example, the left plot shows the gain ratio profiles for +45°, -45°, and the combined Δ90° profile. The right plot displays the measured (blue), corrected (orange), and molecular (reference) VLDR profiles. In this case, the corrected VLDR profile exhibits significant deviations from the molecular values in the aerosol-free regions, indicating calibration inaccuracies. The residual value, representing the difference between the corrected and molecular profiles, is around 0.0054. This residual must be factored into the systematic error for depolarization product assessments, as it impacts the accuracy of polarization measurements.

The second example illustrates an ideal case where the corrected VLDR profile overlaps well over the molecular values in aerosol-free regions. The gain ratio profiles for this case are also consistent, and the residual value is minimal, at just 0.0002. This near-perfect alignment highlights proper calibration, ensuring that polarization measurements are free of significant systematic errors.

These examples underscore the importance of thorough polarization calibration to minimize errors in polarization measurements, particularly when studying properties used for aerosol typing. The comparison between the two cases shows the impact of small residuals on the overall data quality and the necessity of fine-tuning the calibration process to achieve reliable results.

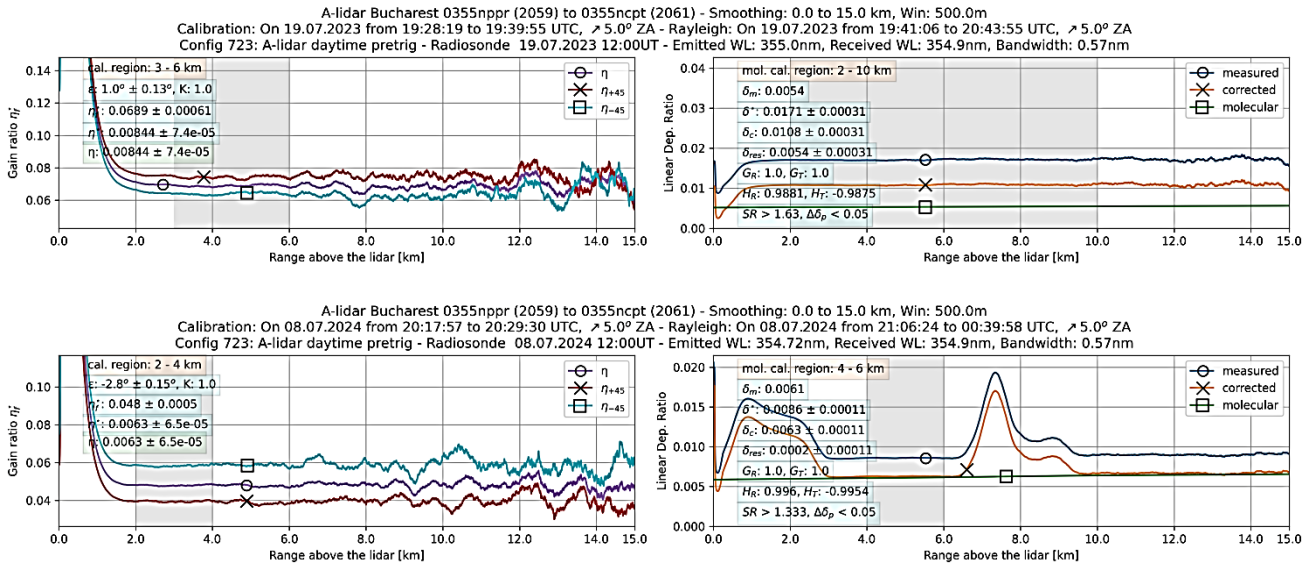


*Fig. 5. Results for the polarization calibration test, collected using the Alpha lidar instrument at 355 nm. Gain ratio profiles on the left and VLDR profiles in the right graph. Upper: corrected VLDR profile (orange) has significant deviations from the molecular values (green). Lower: corrected VLDR profile (orange) overlaps over the molecular depolarization profile (green) (color online)*

The analysis of the Volume Linear Depolarization Ratio (VLDR) systematic errors, derived from polarization calibration tests of the 24 AHLs, shows promising results for most lidar instruments at 532 nm and 355 nm wavelengths (Fig.6). For the majority of cases, the systematic errors are below 0.005, which indicates that these polarization channels are reliable tools for aerosol typing. The low errors in depolarization measurements enhance the capability of lidar systems to differentiate between various aerosol types, contributing to more accurate atmospheric studies.

However, instruments exhibiting systematic errors above 0.005 face significant limitations. In such cases, the uncertainties in lidar depolarization products become too large for reliable aerosol typing, especially in high depolarizing layers, where even small systematic errors can lead to amplified uncertainties. This multiplication effect can distort the interpretation of aerosol properties, reducing the accuracy of aerosol classification.

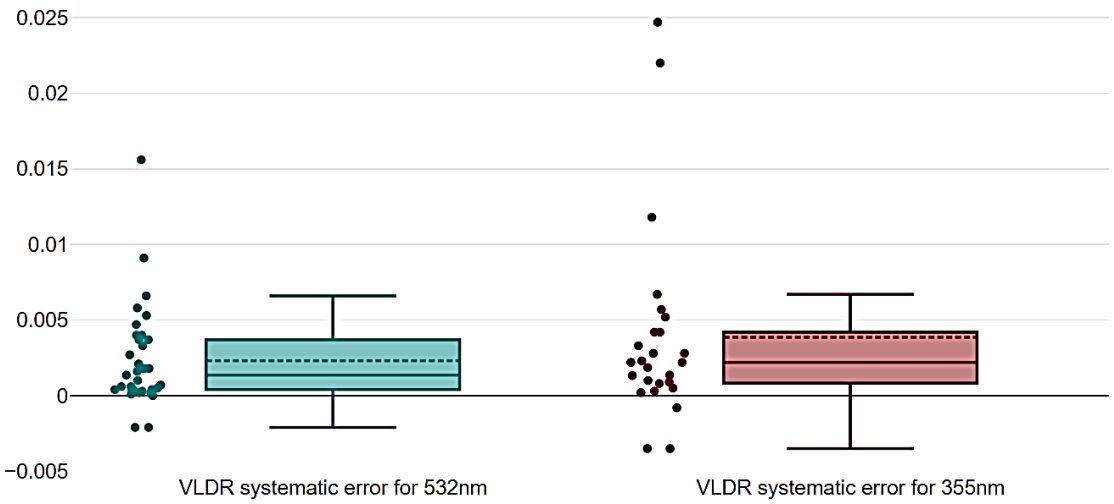


*Fig. 6. Statistical analysis of the VLDR systematic error at 532 nm and 355 nm (color online)*

The results for the 355 nm channel indicate slightly higher uncertainties compared to the 532 nm channel. Graphs show that deviations of the corrected VLDR profiles from the molecular reference values are typically positive, although some case studies reveal negative deviations where the VLDR profile is lower than the molecular profile. Statistically, the mean VLDR systematic error for the 532 nm channel is around 0.0025, while for the 355 nm channel, the mean value is approximately 0.0035.

These findings suggest that, while both channels perform well, the 532 nm channel tends to have slightly more stable and reliable results.

## 4. Conclusions

The results of the QA tests offer valuable insights into the performance of lidar instruments for determining minimum and maximum product heights, as well as the reliability of polarization channels through VLDR systematic error analysis. Most lidar systems show a full overlap altitude between 200 and 1000 m for the 355 nm, 532 nm, and 1064 nm channels, though many do not meet the ACTRIS minimum product height requirement of less than 300 m. Instruments performing at, or above this threshold may require additional near-range telescopes to capture key atmospheric interactions in the lower boundary layer, and to comply with the ACTRIS minimal requirements. The analysis of maximum product heights shows that the 532 nm and 355 nm channels reach a mean maximum altitude of 16 km and 15.7 km, respectively, while the 1064 nm channel is limited to a mean value of 7.4 km, reflecting lower detection capability due to current technical limitations in detector manufacturing for these wavelengths.

For polarization calibration tests, the majority of instruments exhibited VLDR systematic errors below 0.005, particularly for the 532 nm channel, which had a mean error of 0.0025. This indicates a good performance for aerosol typing studies, especially for the 532 nm channel. However, instruments with systematic errors exceeding 0.005 indicate unreliable aerosol classification capabilities, particularly in high depolarizing layers. The 355 nm channel presented slightly higher uncertainties, with a mean systematic error of 0.0035, suggesting the need for further calibration improvements.

Lessons learned during this exercise highlighted that the 532 nm polarization channel outperforms the 355 nm channel, making it more reliable for polarization studies. Additionally, it was evident that significant technical improvements are necessary for the detection systems of the 1064 nm channel to match the performance levels observed in the other channels.

Further analysis on dark and electronic distortions is still ongoing, and additional insights will be presented in a follow-up paper once the necessary processing modules are fully developed. All QA test analyses were conducted using the ATLAS software, developed under the CARS-ACTRIS framework.

**Acknowledgements**

This work was carried out through the Core Program within the National Research Development and Innovation Plan 2022-2027, with the support of MCID, project no. PN 23 05/ 3.01.2023, Ministry of Research, Innovation and Digitization, CCCDI - UEFISCDI, project number PN-III-P1-1.1-TE-2021-0714, within PNCDI III. The research was partially funded by the European Regional Development Fund through the Competitiveness Operational Programme 2014-2020, POC-A.1-A.1.1.1- F- 2015, project Research Centre for Environment and Earth Observation CEO-Terra, SMIS code 108109, contract No. 152/2016. Further support was provided by the European Regional Development Fund through the Competitiveness Operational Programme 2014–2020, Action 1.1.3 Creating synergies with H2020 Programme, project Strengthen the participation of the ACTRIS-RO consortium in the pan-European research infrastructure ACTRIS, ACTRIS-ROC, MYSMIS code 107596 (ctr. no.337/2021). This work was carried out through ATMO-ACCESS project (European Commission

under the Horizon 2020 – Research and Innovation Framework Programme, H2020-INFRAIA-2020-1, Grant Agreement number: 10100800) and CARGO-ACT project (European Commission under the Horizon Europe, HORIZON-INFRA-2023-DEV-01, Grant Agreement number: 101132093).

## References

[1] IPCC 2023, Climate Change 2023: Synthesis Report. Contribution of Working Groups I, II and III to the Sixth Assessment Report of the Intergovernmental Panel on Climate Change [Core Writing Team, H. Lee and J. Romero (eds.)]. IPCC, Geneva, Switzerland, pp. (2023).

[2] S. Solomon, J. Geophys. Res.-Atmos. **112**, 12345 (2007).

[3] R. J. Charlson, S. E. Schwartz, J. M. Hales, R. D. Cess, J. A. Coakley, J. E. Hansen, D. J. Hofmann, Science **255**(5043), 423 (1992).

[4] D. Cimini, V. Rizi, P. Di Girolamo, F. S. Macke, A. Marzano, G. Pappalardo, A. Richter, Atmos. Meas. Tech. **7**, 2981 (2014).

[5] P. Vodička, K. Kawamura, D. K. Deshmukh, P. Pokorná, J. Schwarz, V. Ždímal, Atmospheric Environment **299**, 119619 (2023).

[6] G. Chen, F. Canonaco, A. Tobler, W. Aas, A. Alastuey, J. Allan, A. S. H. Prévôt, Environ. Int. **166**, 107325 (2022).

[7] G. Garnés-Morales, J. P. Montávez, A. Halifa-Marín, P. Jiménez-Guerrero, Atmosphere **14**(3), 491 (2023).

[8] G. Pitari, I. Cionni, G. Di Genova, D. Visioni, I. Gandolfi, E. Mancini, Atmosphere **7**, 149 (2016).

[9] R. Lapere, J. L. Thomas, V. Favier, H. Angot, J. Asplund, A. M. L. Ekman, L. Marelle, J. Raut, A. Da Silva, J. D. Wille, P. Zieger, J. Geophys. Res.-Atmos. **129**(2), (2024).

[10] L. Mona, F. Marenco, Elsevier eBooks, 161 (2016).

[11] D. L. Hartmann, M. E. Ockert-Bell, M. L. Michelsen, J. Climate **5**, 1281 (1992).

[12] M. O. Andreae, C. D. Jones, P. M. Cox, Nature **435**(7046), 1187 (2005).

[13] S. J. Gonçalves Jr., H. Evangelista, J. Weis, T. H. Harder, S. China, S. Müller, M. M. Marques, N. de Magalhães Neto, H. R. Passos, M. Sampaio, J. C. Simões, Bruno V. X. de Oliveira, C. I. Yamamoto, A. Laskin, M. K. Gilles, R. H. M. Godoi, Commun. Earth Environ. **4**, 77 (2023).

[14] S. Yook, D. W. J. Thompson, S. Solomon, Geophys. Res. Lett. **49**(10), (2022).

[15] A. Ansmann, K. Ohneiser, A. Chudnovsky, D. A. Knopf, E. W. Eloranta, D. Villanueva, P. Seifert, M. Radenz, B. Barja, F. Zamorano, C. Jimenez, R. Engelmann, H. Baars, H. Griesche, J. Hofer, D. Althausen, U. Wandinger, Atmos. Chem. Phys. **22**(17), 11701 (2022).

[16] https://www.actris.eu/topical-centre/cars/announcements-resources/documents

[17] P. Laj, C. L. Myhre, V. Riffault, V. Amiridis, H. Fuchs, K. Eleftheriadis, T. Petäjä, T. Salameh, N. Kivekäs, E. Juurola, G. Saponaro, S. Philippin, C. Cornacchia, L. A. Arboledas, H. Baars, A. Claude, M. De Mazière, B. Dils, M. Dufresne, N. Evangeliou, O. Favez, M. Fiebig, M. Haeffelin, H. Herrmann, K. Höhler, N. Illmann, A. Kreuter, E. Ludewig, E. Marinou, O. Möhler, L. Mona, L. E. Murberg, D. Nicolae, A. Novelli, E. O'Connor, K. Ohneiser, R. M. Petracca Altieri, B. Picquet-Varrault, D. van Pinxteren, B. Pospichal, J-P Putaud, S. Reimann, N. Siomos, I. Stachlewska, R. Tillmann, K. Artemis Voudouri, U. Wandinger, A. Wiedensohler, A. Apituley, A. Comerón, M. Gysel-Beer, N. Mihalopoulos, N. Nikolova, A. Pietruczuk, S. Sauvage, J. S. H. Skov, T. Svendby, E. Swietlicki, D. Tonev, G. Vaughan, V. Zdimal, U. Baltensperger, J-F Doussin, M. Kulmala, G. Pappalardo, S. Sorvari Sundet, M. Vanaar, Bull. Am. Meteorol. Soc. **105**(7), E1098 (2024).

[18] V. Nicolae, L. Belegante, J. Vasilescu, A. Nemuc, F. Toanca, O. G. Tudose, C. Radu, D. Nicolae, J. Optoelectron. Adv. M. **25**(3-4), 176 (2023).

[19] M. Wiegner, I. Mattis, M. Pattantyús-Ábrahám, J. A. Bravo-Aranda, Y. Poltera, A. Haefele, M. Hervo, U. Görsdorf, R. Leinweber, J. Gasteiger, M. Haeffelin, F. Wagner, J. Cermak, K. Komínková, M. Brettle, C. Münkel, K. Pönitz, Atmos. Meas. Tech. **12**, 471 (2019).

[20] S. Kotthaus, J. A. Bravo-Aranda, M. Collaud Coen, J. L. Guerrero-Rascado, M. J. Costa, D. Cimini, E. J. O'Connor, M. Hervo, L. Alados-Arboledas, M. Jiménez-Portaz, L. Mona, D. Ruffieux, A. Illingworth, M. Haeffelin, Atmos. Meas. Tech. **16**, 433 (2023).

[21] A. Ansmann, D. Müller, Lidar: Range-Resolved Optical Remote Sensing of the Atmosphere **102**, Springer, 105 (2005).

[22] D. Müller, U. Wandinger, D. Althausen, I. Mattis, A. Ansmann, Appl. Opt. **37**, 2260 (1998).

[23] A. A. Floutsi, H. Baars, R. Engelmann, D. Althausen, A. Ansmann, S. Bohlmann, B. Heese, J. Hofer, T. Kanitz, M. Haarig, K. Ohneiser, M. Radenz, P. Seifert, A. Skupin, Z. Yin, S. F. Abdullaev, M. Komppula, M. Filioglou, E. Giannakaki, I. S. Stachlewska, L. Janicka, D. Bortoli, E. Marinou, V. Amiridis, A. Gialitaki, R-E Mamouri, B. Barja, U. Wandinger, Atmos. Meas. Tech. **16**, 2353 (2023).

[24] I. Mattis, G. D'Amico, H. Baars, A. Amodeo, F. Madonna, M. Iarlori, Atmos. Meas. Tech. **9**, 3009 (2016).

[25] S. P. Burton, R. A. Ferrare, C. A. Hostetler, J. W. Rogers R. R. Hair, M. D. Obland, C. F. Butler, A. L. Cook, D. B. Harper, K. D. Froyd, Atmos. Meas. Tech. **5**, 73 (2012).

[26] D. Nicolae, J. Vasilescu, C. Talianu, I. Binietoglou, V. Nicolae, S. Andrei, B. Antonescu, Atmos. Chem. Phys. **18**, 14511 (2018).

[27] U. Wandinger, A. A. Floutsi, H. Baars, M. Haarig, A. Ansmann, A. Hünerbein, N. Docter, D. Donovan,

G.-J. van Zadelhoff, S. Mason, J. Cole, Atmos. Meas. Tech. **16**, 2485 (2023).
[28] V. Freudenthaler, H. Linné, A. Chaikovski, D. Rabus, S. Groß, Atmos. Meas. Tech. Discuss. (in review) (2018).
[29] P. Paschou, N. Siomos, A. Tsekeri, A. Louridas, G. Georgoussis, V. Freudenthaler, I. Binietoglou, G. Tsaknakis, A. Tavernarakis, C. Evangelatos, J. von Bismarck, T. Kanitz, C. Meleti, E. Marinou, V. Amiridis, Atmos. Meas. Tech. **15**, 2299 (2022).
[30] R. M. Pauly, J. E. Yorks, D. L. Hlavka, M. J. McGill, V. Amiridis, S. P. Palm, S. D. Rodier, M. A. Vaughan, P. A. Selmer, A. W. Kupchock, H. Baars, A. Gialitaki, Atmos. Meas. Tech. **12**, 6241 (2019).
[31] M. Vaughan, A. Garnier, D. Josset, M. Avery, K.-P. Lee, Z. Liu, W. Hunt, J. Pelon, Y. Hu, S. Burton, J. Hair, J. L. Tackett, B. Getzewich, J. Kar, S. Rodier, Atmos. Meas. Tech. **12**, 51 (2019).
[32] V. Freudenthaler, EARLINET-ASOS 7th workshop, available at: https://epub.ub.uni-muenchen.de/12970/ (2009).
[33] L. Belegante, J. A. Bravo-Aranda, V. Freudenthaler, D. Nicolae, A. Nemuc, D. Ene, L. Alados-Arboledas, A. Amodeo, G. Pappalardo, G. D'Amico, F. Amato, R. Engelmann, H. Baars, U. Wandinger, A. Papayannis, P. Kokkalis, S. N. Pereira, Atmos. Meas. Tech. **11**, 1119 (2018).
[34] G. Pappalardo, A. Amodeo, A. Apituley, A. Comeron, V. Freudenthaler, H. Linné, A. Ansmann, J. Bösenberg, G. D'Amico, I. Mattis, L. Mona, U. Wandinger, V. Amiridis, L. Alados-Arboledas, D. Nicolae, M. Wiegner, Atmos. Meas. Tech. **7**, 2389 (2014).
[35] E. Giannakaki, P. Kokkalis, E. Marinou, N. S. Bartsotas, V. Amiridis, A. Amsmann, M. Kompulla, Atmos. Meas. Tech. **13**, 893 (2020).
[36] U. Wandinger, V. Freudenthaler, H. Baars, A. Amodeo, R. Engelmann, I. Mattis, S. Groß, G. Pappalardo, A. Giunta, G. D'Amico, A. Chaikovsky, F. Osipenko, A. Slesar, D. Nicolae, L. Belegante, C. Talianu, I. Serikov, H. Linné, F. Jansen, A. Apituley, K. M. Wilson, M. de Graaf, T. Trickl, H. Giehl, M. Adam, A. Comerón, C. Muñoz-Porcar, F. Rocadenbosch, M. Sicard, S. Tomás, D. Lange, D. Kumar, M. Pujada, F. Molero, A. J. Fernández, L. Alados-Arboledas, J. A. Bravo-Aranda, F. Navas-Guzmán, J. L. Guerrero-Rascado, M. J. Granados-Muñoz, J. Preißler, F. Wagner, M. Gausa, I. Grigorov, D. Stoyanov, M. Iarlori, V. Rizi, N. Spinelli, A. Boselli, X. Wang, T. Lo Feudo, M. R. Perrone, F. De Tomasi, P. Burlizzi, Atmos. Meas. Tech. **9**, 1001 (2016).
[37] J. A. Bravo-Aranda, L. Belegante, V. Freudenthaler, L. Alados-Arboledas, D. Nicolae, M. J. Granados-Muñoz, J. L. Guerrero-Rascado, A. Amodeo, G. D'Amico, R. Engelmann, G. Pappalardo, P. Kokkalis, R. Mamouri, A. Papayannis, F. Navas-Guzmán, F. José Olmo, U. Wandinger, F. Amato, M. Haeffelin, Atmos. Meas. Tech. **9**, 4935 (2016).
[38] V. Freudenthaler, Atmos. Meas. Tech. **9**, 4181 (2016).
[39] https://github.com/nikolaos-siomos/ATLAS
[40] G. D'Amico, A. Amodeo, I. Mattis, V. Freudenthaler, G. Pappalardo: Atmos. Meas. Tech. **9**, 491 (2016).
[41] I. Mattis, G. D'Amico, H. Baars, A. Amodeo, F. Madonna, M. Iarlori, Atmos. Meas. Tech. **9**, 3009 (2016).
[42] G. David, A. Miffre, B. Thomas, P. Rairoux, Appl. Phys. B **108**, 197 (2012).
[43] V. Freudenthaler, M. Esselborn, M. Wiegner, B. Heese, M. Tesche, A. Ansmann, D. Müller, D. Althausen, M.,Wirth, A. Fix, G. Ehret, P. Knippertz, C. Toledano, J. Gasteiger, M. Garhammer, M. Seefeldner, Tellus B **61**, 165 (2009).
[44] https://www.actris.eu/news-events/news/first-intercomparison-campaign-cars-reference-lidar-systems-has-started-mars
[45] https://environment.inoe.ro/article/221/multiwavelength-raman-lidar-rali
[46] D. Nicolae, A. Nemuc, D. Müller, C. Talianu, J. Vasilescu, L. Belegante, A. Kolgotin, J. Geophys. Res. Atmos. **118**, 2956 (2013).
[47] L. Belegante, M. M. Cazacu, A. Timofte, F. Toanca, J. Vasilescu, M. I. Rusu, N. Ajtai, H. I. Stefanie, I. Vetres, A. Ozunu, S. Gurlui, Environmental Engineering and Management Journal **14**(11), 2503 (2015).

*Corresponding author: camelia@inoe.ro